Multiple higher-order singularities and iso-dynamics in a simple glass-former model

Nicoletta Gnan[1], Gayatri Das[2], Matthias Sperl[3], Francesco Sciortino[2] and Emanuela Zaccarelli[1,2]
[1] *CNR-ISC Uos Sapienza, Piazzale A. Moro 2, I-00185, Roma, Italy*
[2] *Dipartimento di Fisica, Sapienza Università di Roma, Piazzale A. Moro 2, I-00185, Roma, Italy and*
[3] *Institut für Materialphysik im Weltraum, Deutsches Zentrum für Luft-und Raumfahrt, 51170 Köln, Germany*
(Dated: July 16, 2014)

We investigate the slow dynamics of a colloidal model with two repulsive length scales, whose interaction potential is the sum of a hard-core and a square shoulder. Despite the simplicity of the interactions, Mode-Coupling theory predicts a complex dynamic scenario: a fluid-glass line with two reentrances and a glass-glass line ending with multiple higher-order (A_3 or A_4) singularities. In this work we verify the existence of the two A_4 points by numerical simulations, observing subdiffusive behaviour of the mean-square displacement and logarithmic decay of the density correlators. Surprisingly, we also discover a novel dynamic behaviour generated by the competition between the two higher-order singularities. This results in the presence of special loci along which the dynamics is identical *at all* length and time scales.

arXiv:1407.3917v1 [cond-mat.soft] 15 Jul 2014

Introduction: Colloidal solutions often display a rich variety of dynamical behaviour. Experiments have shown that the addition of a short-range attraction to the excluded volume interaction generates multiple dynamically arrested (glassy) states, explored by tuning the interaction strength, the packing fraction or the range of the attraction[1–6]. These experimental studies have confirmed predictions based on the Mode Coupling Theory (MCT) [7–11] and numerical simulations [4, 12–15, 17]. Unconventional dynamics have also been reported for purely repulsive colloidal mixtures. In particular, multiple glasses have been found in binary mixtures of hard [18, 19] and soft spheres[20–22]. Also in star-polymer mixtures, distinct glasses have been found to surround a region of ergodic state points [23, 24]. In all these cases, different microscopic mechanisms compete to generate multiple arrested states.

Recently, core softened potentials with two repulsive length scales have been identified as good candidates for displaying novel glassy dynamics. These models have been used to describe systems ranging from metallic glasses [25] to granular materials [26], as well as silica [27], water [28, 29] and penetrable soft particles such as diblock copolymers, dendritic polymers, vesicles or microgels [30–33]. The square-shoulder (SS) model, i.e. a model system whose interaction potential is a hard-core repulsion of extent σ complemented by a repulsive shoulder, belongs to the family of core-softened potentials. For the SS model MCT calculations have predicted the existence of multiple glass transitions [34]. Indeed, for specific values of the shoulder width Δ, the temperature T-packing fraction ϕ state diagram is characterized by a non-monotonic fluid-glass transition line, retracing both upon cooling and upon compression.The peculiar MCT predictions for the SS is the additional presence of a glass-glass line for small enough Δ terminating with two A_3 singularities, fully embedded within the glass phase as shown in the schematic Fig. 1 (a). Upon increasing Δ, the glass-glass line progressively moves towards the fluid-glass one and the two eventually merge (Fig.1 (b),(c)). When the A_3 point collides with the fluid-glass line, MCT predicts the presence of a higher-order singularity, named A_4. The dynamics close to higher order singularities differs from the standard fluid-glass scenario. Instead of the characteristic two-step dynamics, the decay of the density correlators shows a logarithmic dependence on time t. Correspondingly, the mean-squared displacement (MSD) shows a subdiffusive behaviour, i.e. $\sim t^a$ with $a < 1$[11]. Similar features have been observed also in theoretical studies on facilitated models[35], confirming the robustness of MCT results.

Despite the novelty of these MCT predictions, the observation of the peculiar dynamic behavior of the SS model, associated to higher-order singularities, has been difficult to achieve [36]. Indeed, the A_3 points are buried in the glass region and hence can not be accessed via an ergodic path. Differently, the A_4 can be approached from the fluid (ergodic) side and hence its role can be explored in equilibrium. In addition, since the SS model is characterized by two A_3 points, it should have two distinct A_4 points (see Fig.1 (b),(c)). In this Letter we provide numerical evidence of the existence of two A_4 singularities in the SS model, by observing subdiffusive behaviour of the MSD and logarithmic decay of the density correlators for several time decades. Additionally, we find a novel dynamic behaviour that occurs in the fluid region, generated by the interplay of the two closeby higher-order points. We discover that their simultaneous presence gives rise to special loci in the $T-\phi$ plane along which the dynamics is identical (*iso-dynamics* loci), i.e. where both the short- and the long-time dynamics of the system remarkably coincide *at all* length scales.

Model and Methods: We perform event-driven molecular dynamics simulations of a 50 : 50 non-crystallising binary mixture of $N = 2000$ particles of species A and B

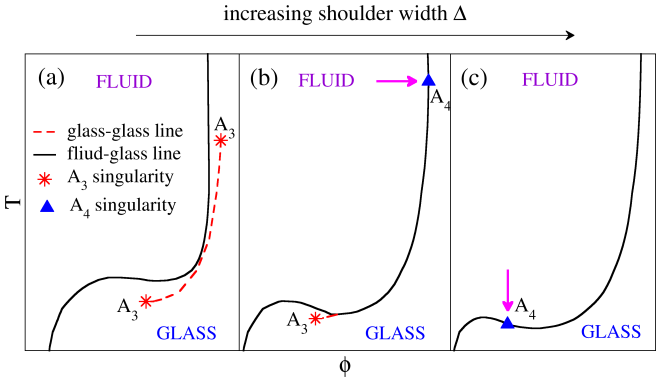

FIG. 1. Schematic evolution of the MCT dynamic state diagram of the SS system for increasing values of the shoulder width Δ. (a) For small Δ, beside the fluid-glass line (solid line), a disconnected glass-glass line is predicted (dashed line), ending in two A_3 higher-order singularities (stars). (b) On increasing Δ, the glass-glass line merges with the fluid-glass line and an A_4 singularity appears when one of the two A_3 points meets the fluid-glass line (filled triangle). (c) At even larger Δ also the second A_3 point eventually intersects the fluid-glass line generating a distinct A_4 higher-order singularity (filled triangle). The arrows in (b) and (c) indicate the paths followed to locate the A_4 singularities in the simulations.

interacting via the pairwise SS potential

$$V_{ij}(r) = \begin{cases} \infty, & r < \sigma_{ij} \\ u_0, & \sigma_{ij} \le r < (1+\Delta)\sigma_{ij} \\ 0, & r \ge (1+\Delta)\sigma_{ij}, \end{cases} \qquad (1)$$

where $i,j = A,B$, σ_{ij} is the hard core between two particles, Δ is the shoulder width, and u_0 is the shoulder height. The size ratio between the two species is $\sigma_{AA}/\sigma_{BB} = 1.2$ and $\sigma_{AB} = (\sigma_{AA}+\sigma_{BB})/2$. The mass of particles is $m = 1$. σ_{BB} and u_0 are chosen as units of length and energy, so that the time t is measured in units of $t_0 = \sigma_{BB}\sqrt{m/u_0}$. T is measured in units of energy (k_B=1). Simulations are performed in the canonical and microcanonical ensemble for a wide range of T and $\phi = (\pi/6)(\rho_A\sigma_{AA}^3 + \rho_B\sigma_{BB}^3)$, where $\rho_A = \rho_B = \rho/2$, $\rho \equiv N/V$ with V the volume of the cubic simulation box.

To locate the higher-order singularities we perform an extensive study of the dynamics of the SS system. Building on the previous study for $\Delta = 0.15$ [36], where comparison between simulations and theoretical predictions have provided an estimate of the A_3 points, we restricted our search of the two A_4 points to values of $\Delta \ge 0.17$. Specifically, we have analyzed in depth the range $0.17 \le \Delta \le 0.24$, with a mesh of 0.01. For each Δ we have studied the dynamics in a wide window of ϕ and T. Such lengthy investigation has allowed us to locate the first $A_4^{(1)}$ singularity at the state point ($\phi^{*(1)} \simeq 0.6$, $T^{*(1)} \simeq 0.55$, $\Delta^{*(1)} \simeq 0.21$) and the second $A_4^{(2)}$ at ($\phi^{*(2)} \simeq 0.4$, $T^{*(2)} \simeq 0.15$, $\Delta^{*(2)} \simeq 0.24$). Details of this procedure, based on the mapping of the MCT prediction onto the numerical data, are provided in the Supplementary Material.

Dynamics close to the two A_4 singularities: Figure 2 shows the dynamic behaviour of the system close to the two A_4 singularities. In the case of $A_4^{(1)}$ (top row panels) we follow the evolution of dynamic quantities on changing ϕ at $\Delta^{*(1)}$ and $T^{*(1)}$ fixed, while for $A_4^{(2)}$ (bottom row panels) we work at fixed $\Delta^{*(2)}$ and $\phi^{*(2)}$ upon changing T, following the paths highlighted in Fig. 1 (b) and (c). Fig. 2(a) shows the increasing subdiffusive behaviour of the MSD for the A particles $\langle \delta r_{AA}^2 \rangle$ on increasing ϕ which extends up to three orders of magnitude at $\phi = 0.6$. The B particles behave likewise (inset of Fig. 2(a)). The collective density correlators $\Phi_q^{AA}(t)$ of the A particles display similarly striking features. This is shown in Figure 2 (b) where the correlators are reported for several wave-vectors $q\sigma_{AA}$. For a large time window the decay of $\Phi_q^{AA}(t)$ is well described by a second degree polynomial in $\ln(t)$, i.e. $\Phi_q^{AA}(t) \sim f_q - H_q^{(1)} \ln(t/\tau) + H_q^{(2)} \ln(t/\tau)^2$, where f_q, $H_q^{(1)}$,$H_q^{(2)}$ are fit parameters. For a special wavevector $q^{*(1)}$, $H_q^{(2)} \sim 0$ and the correlator displays a pure logarithmic decay. We find $q^{*(1)}\sigma_{AA} = 15.5$. In addition, in the q-vector region explored we observe the convex-to-concave crossover predicted by MCT[11]. The ϕ dependence of $\Phi_q^{AA}(t)$, reported in Fig. 2 (c), shows the growth of the logarithmic regime on approaching $A_4^{(1)}$.

The same analysis has been carried out for $A_4^{(2)}$. As shown in Fig.1 (c), such singularity lays close to the reentrance, which makes it difficult to explore the region around it by moving along constant T paths. In addition, even along the constant ϕ path (i.e. by varying T) the presence of a re-entrant fluid-glass line (imposing its two-step relaxation behavior) partially interferes with the logarithmic dynamics induced by the A_4 point. As a result, dynamical quantities in Fig. 2 (d)-(f) look different from those obtained for the $A_4^{(1)}$. Figure 2 (d) shows $\langle \delta r_{AA}^2 \rangle$ as a function of T for the A and B (inset) particles. In this case the subdiffusive region is preceded by a plateau, a signature of the standard caging effect imposed by the nearby liquid-glass line. The subdiffusive region, the hallmark of the higher-order singularity, is shifted to higher times and extends over almost three decades. The interplay between the fluid-glass line and the A_4 dynamics is also observable in the decay of $\Phi_q^{AA}(t)$ at ($\phi^{*(2)}$, $T^{*(2)}$, $\Delta^{*(2)}$) in Fig. 2(e). For all q-vectors the initial part of the structural relaxation displays the typical two-step behavior, but, for longer times, the decay becomes logarithmic. We find a pure logarithmic behaviour in $\Phi_q^{AA}(t)$ for $q^{*(2)}\sigma_{AA} = 13.6$. The evolution of $\Phi_q^{AA}(t)$ at $q^{*(2)}\sigma_{AA}$ with T is shown in Fig. 2(f): the long time decay becomes more and more linear in $\ln(t)$ on approaching $A_4^{(2)}$.

Iso-dynamics lines: The procedure to locate the A_4 singularities required the investigation of a very large

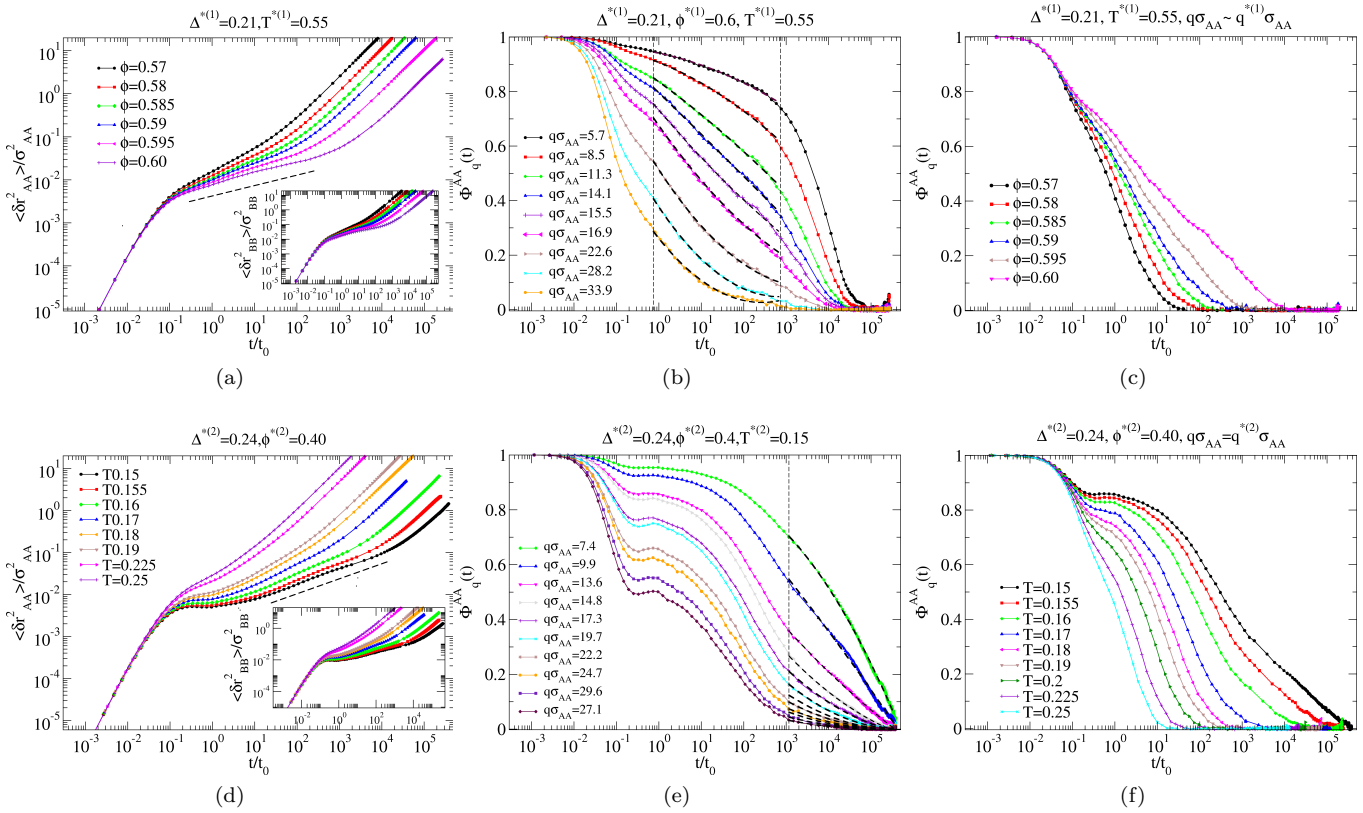

FIG. 2. Dynamical quantities close to the two higher-order singularities $A_4^{(1)} \equiv (\phi^{*(1)} \simeq 0.6, T^{*(1)} \simeq 0.55, \Delta^{*(1)} \simeq 0.21)$ and $A_4^{(2)} \equiv (\phi^{*(2)} \simeq 0.4, T^{*(2)} \simeq 0.15, \Delta^{*(2)} \simeq 0.24)$, along paths shown in Fig.1 (b) and (c) respectively. (a) A-particles MSD as a function of the scaled time t_0 for different ϕ at $T^{*(1)}, \Delta^{*(1)}$. The dashed line is a power-law ($\propto t^{0.3}$) to highlight the subdiffusive regime. The inset shows the MSD for the B species. (b) Collective density correlators of the A species $\Phi_q^{AA}(t)$ evaluated at $A_4^{(1)}$ for different wave vectors $q\sigma_{AA}$. The dotted vertical lines delimit the time window in which $\Phi_q^{AA}(t)$ display a logarithmic behaviour. (c) $\Phi_q^{AA}(t)$ at $T^{*(1)}, \Delta^{*(1)}$ as a function of ϕ. (d) MSD for A particles at $T^{*(2)}, \Delta^{*(2)}$ as function of the scaled time t_0 for different T. The subdiffusive regime is characterised by $\propto t^{0.37}$. Inset: MSD of B particles. (e) The same as (b) but evaluated at the $A_4^{(2)}$. Despite the interference of the fluid-glass line on the dynamics (see text), a long time logarithmic behaviour can be identified. (f)$\Phi_{q^{*(2)}}^{AA}(t)$ at $\phi^{*(2)}, \Delta^{*(2)}$ as a function of T.

number of state points for several Δ values. During such process, we have discovered a peculiar dynamic feature of the SS model that we associate to the simultaneous presence of two distinct higher order singularities (A_3 or A_4). Specifically, we find that the competition between these two special points generates loci in the T-ϕ plane with invariant dynamics, that we name iso-dynamics lines. To gain a deeper understanding of such loci we investigate in details the region in between two A_3 singularities for $\Delta = 0.17$, i.e. for the case schematically shown in Fig. 1(b). We focus on iso-diffusivity (iso-D/D_0)[14] paths close to the fluid-glass line ($D_0 \equiv \sigma_{BB}^2/t_0$ accounts for the trivial effect of the thermal velocity), as shown in the inset of Fig.3(a). Surprisingly, we find that state points along iso-D/D_0 curves are characterized not only by the same long-time dynamics but also by the same short and intermediate time dependence. Figures 3(a) and (b) show, respectively, the MSD and $\Phi_q^{AA}(t)$ as a function of t/t_0, along three iso-D/D_0 lines, differing by more than two orders of magnitude in D/D_0. For all three iso-D/D_0 sets, the superposition of the curves, *at all times* and *at all length scales* is striking, both in real and in Fourier space. To further support the iso-dynamics behavior at all length scales we show in Fig. 4(a) the wave-vector dependence of $\Phi_q^{AA}(t)$ for a specific value of D/D_0. Again, superposition of the correlation functions at all times is observed for all q values. These results prove the existence of iso-dynamics loci, i.e. lines in the $T-\phi$ plane where an identical dynamics is observed. It is interesting to notice that while dynamics is identical, structural and thermodynamic properties are not, as discussed in the Supplementary Material. Finally we remark that only state points that feel the presence of both higher order singularities obey the invariance. Fig. 4(b) shows that the decay of $\Phi_q^{AA}(t)$ does not satisfy the invariance for T and ϕ progressively moving closer

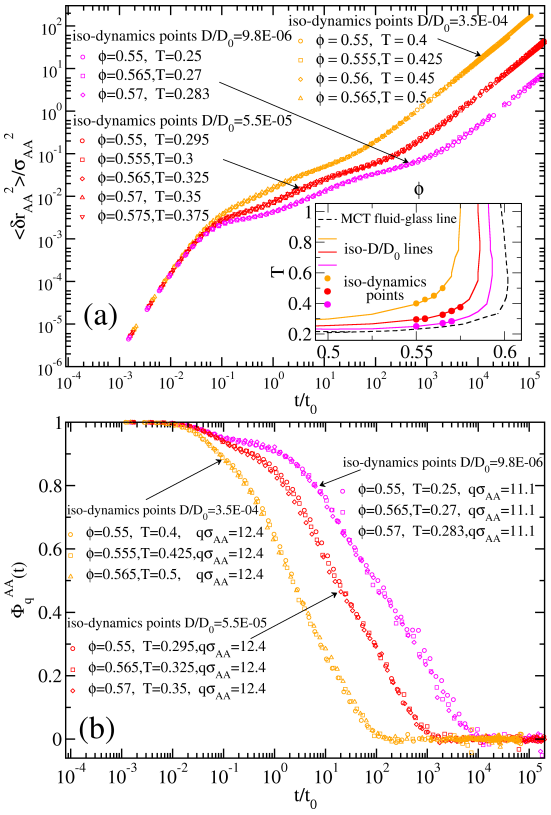

FIG. 3. Dynamical properties for $\Delta = 0.17$ along three iso-dynamics lines with rescaled diffusivity $D/D_0 = 3.5 \times 10^{-4}$ (orange symbols), $D/D_0 = 5.5 \times 10^{-5}$ (red symbols) and $D/D_0 = 9.8 \times 10^{-6}$ (magenta symbols). (a) MSD of the A species along the iso-dynamics line as a function of t/t_0 (b) Density correlator for the same sets of iso-dynamics points in (a) as a function of t/t_0. The inset shows the position of the iso-D/D_0 lines and of the expected fluid-glass line (see Supplementary Material).

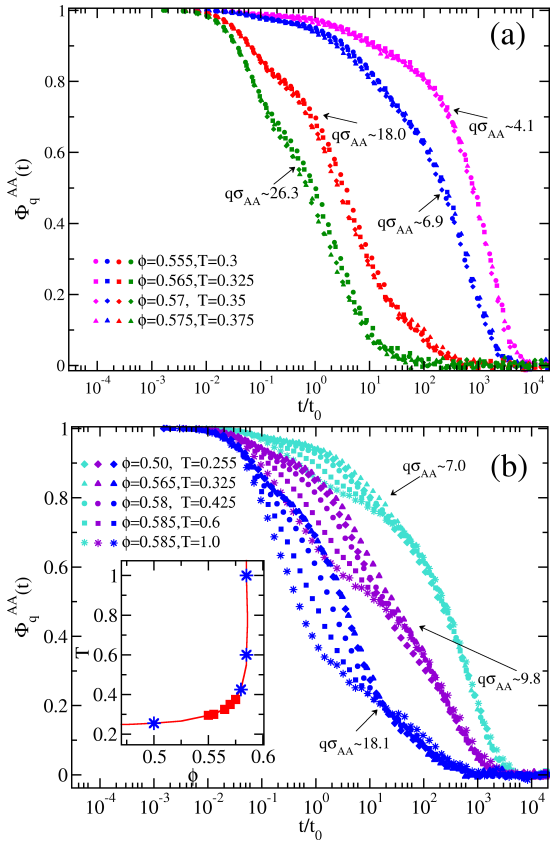

FIG. 4. $\Phi_q^{AA}(t)$ along the iso-$D/D_0 = 5.5 \times 10^{-5}$ line for $\Delta = 0.17$ at different wave vectors $q\sigma_{AA}$ for (a) iso-dynamics and (b) non iso-dynamics state points. The inset shows the location of such points in the T-ϕ diagram. Squares/stars indicate iso-dynamics/non iso-dynamics points.

to one singularity (but always on the iso-D/D_0 line). In this case, while the long time dynamics is identical (as one could expect on the basis of the identical diffusion coefficient), the short and intermediate time dynamics is now clearly different, indicating that the system explores the nearest-neighbour cages in a different way for each state point. The state points where the iso-dynamics is/is-not observed are indicated in the inset of Fig. 4(b). In the Supplementary Material, we discuss how the iso-dynamics behaviour is compatible with MCT predictions.

Conclusions: We have reported numerical evidence of the existence of two A_4 singularities in a simple system with two repulsive length scales. We have confirmed that anomalous dynamical features, such as the logarithmic decay of the density autocorrelation function and the subdiffusive regime in the mean-square displacement, characterize the dynamics close to these points. This result provides (i) one of the most stringent test of previously formulated MCT predictions (ii) evidence that soft-colloidal particles could constitute a model system for experimentally testing these highly unconventional behavior. In addition, we unexpectedly discovered that the competition between two higher-order singularities gives rise to a non-trivial iso-dynamics in between the two singularities. Such state points share the same dynamics at all time and length-scales. We hope our study will stimulate the experimental search for anomalous dynamics and competing glass transitions in core-softened systems and in repulsive systems with two competing length scales.

Acknowledgments NG, EZ acknowledge support from MIUR ("Futuro in Ricerca" ANISOFT/RBFR125H0M); GD, FS, EZ from EU ITN-234810-COMPLOIDS.

[1] F. Mallamace, P. Gambadauro, N. Micali, P. Tartaglia, C. Liao, and S. H. Chen, Phys. Rev. Lett. **84**, 5431 (2000).
[2] T. Eckert and E. Bartsch, Phys. Rev. Lett. **89**, 125701 (2002).
[3] K. N. Pham, A. M. Puertas, J. Bergenholtz, S. U. Egelhaaf, A. Moussaïd, P. N. Pusey, A. B. Schofield, M. E. Cates, M. Fuchs, and W. C. K. Poon, Science **296**, 104 (2002).

[4] S. H. Chen, W.-R.Chen, and F. Mallamace, Science **300**, 619 (2003).
[5] K. N. Pham, S. U. Egelhaaf, P. N. Pusey, and W. C. K. Poon, Phys. Rev. E **69**, 1 (2004).
[6] X. Lu, S. G. J. Mochrie, S. Narayanan, A. R. Sandy, and M. Sprung, Phys. Rev. Lett. **100**, 045701 (2008).
[7] W. Götze, *Complex Dynamics of Glass-Forming Liquids: A Mode-Coupling Theory* (Oxford Univ Press, New York, 2009).
[8] L. Fabbian, W. Götze, F. Sciortino, P. Tartaglia, and F. Thiery, Phys. Rev. E **59**, 1347 (1999).
[9] J. Bergenholtz and M. Fuchs, Phys. Rev. E **59**, 5706 (1999).
[10] K. A. Dawson, G. Foffi, M. Fuchs, W. Götze, F. Sciortino, M. Sperl, P. Tartaglia, T. Voigtmann, and E. Zaccarelli, Phys. Rev. E **63**, 011401 (2001).
[11] W. Götze and M. Sperl, Phys. Rev. E **66**, 011405 (2002).
[12] A. M. Puertas, M. Fuchs, and M. E. Cates, Phys. Rev. Lett. **88**, 098301 (2002).
[13] G. Foffi, K. A. Dawson, S. V. Buldyrev, F. Sciortino, E. Zaccarelli, and P. Tartaglia, Phys. Rev. E **65**, 050802 (2002).
[14] E. Zaccarelli, G. Foffi, K. A. Dawson, S. V. Buldyrev, F. Sciortino, and P. Tartaglia, Phys. Rev. E **66**, 041402 (2002).
[15] A. Puertas, M. Fuchs, and M. E. Cates, Phys. Rev. E **67**, 031406 (2003).
[4] F. Sciortino, P. Tartaglia, and E. Zaccarelli, Phys. Rev. Lett. **91**, 268301 (2003).
[17] E. Zaccarelli, F. Sciortino, and P. Tartaglia, J. Phys.: Condens. Matter **16**, 4849 (2004).
[18] A. Imhof and J. K. G. Dhont, Phys. Rev. Lett. **75**, 1662 (1995).
[19] T. Voigtmann, Europhys. Lett. **96**, 36006 (2011).
[20] A. J. Moreno and J. Colmenero, Phys. Rev. E **74**, 021409 (2006).
[21] A. J. Moreno and J. Colmenero, J. Chem. Phys. **125**, 164507 (2006).
[22] T. Voigtmann and J. Horbach, Phys. Rev. Lett. **103**, 205901 (2009).
[23] C. Mayer, E. Zaccarelli, E. Stiakakis, C. N. Likos, F. Sciortino, A. Munam, M. Gauthier, N. Hadjichristidis, H. Iatrou, P. Tartaglia, et al., Nat. Mater. **7**, 780 (2008).
[24] C. Mayer, F. Sciortino, C. N. Likos, P. Tartaglia, H. Loewen, and E. Zaccarelli, Macromolecules **42**, 423 (2009).
[25] D. A. Young and B. J. Alder, Phys. Rev. Lett. **38**, 1213 (1977).
[26] J. Duran, *Sands and Powders and Grains: An Introduction to the Physics of Granular Materials* (Springer, New York, 1999).
[27] Y. D. Fomin and E. N. Tsiok, Phys. Rev. E **87**, 042122 (2013).
[28] E. A. Jagla, J. Chem. Phys. **111**, 8980 (1999).
[29] A. de Oliveira, P. A. Netz, and B. M. C., Eur. Phys. J. B **64**, 481 (2008).
[30] P. Ziherl and R. D. Kamien, Phys. Rev. Lett. **85**, 3528 (2000).
[31] G. Malescio and G. Pellicane, Nat. Mater. **2**, 97 (2003).
[32] N. Osterman, D. Babic, I. Poberaj, J. Dobnikar, and P. Ziherl, Phys. Rev. Lett. **99**, 248301 (2007).
[33] T. Dotera, T. Oshiro, and P. Ziherl, Nature **506**, 208 (2014).
[34] M. Sperl, E. Zaccarelli, F. Sciortino, P. Kumar, and H. E. Stanley, Phys. Rev. Lett. **104**, 145701 (2010).
[35] M. Sellitto, J. Chem Phys. **138**, 224507 (2013).
[36] G. Das, N. Gnan, F. Sciortino, and E. Zaccarelli, J. Chem. Phys. **138**, 134501 (2013).

MAPPING OF MCT FLUID-GLASS LINE ON SIMULATION DATA

To investigate the presence of two A_4 points, we solve the MCT for the monodisperse SS system finding the presence of the two higher-order singularities within the Rogers-Young (RY) closure. These predictions have been confirmed by repeating the MCT calculations for our binary mixture, using as input of the theory the structure factors $S(q)$ evaluated in simulations, thus avoiding to rely on a specific closure of the Ornstein-Zernike equation. From these calculations we estimate $\Delta^{*(1)}_{MCT} \simeq 0.17$ and $\Delta^{*(2)}_{MCT} \simeq 0.20$. As already observed in previous works, the MCT gives a qualitative, but not quantitative, estimation of the fluid-glass line and of higher-order singularities. Hence, to correctly locate the A_4 we need to map the theoretical fluid-glass line on that extrapolated from simulations. The latter can be achieved from a well established procedure: we perform simulations for several state points at intermediate and low diffusivities in order to extract the diffusion coefficient D of the species A from the long-time limit of the mean-square displacement. On approaching the ideal glass line MCT predicts that D tends to zero following the laws $D \sim \mid \phi - \phi_g(T) \mid^{\gamma(T)}$ and $D \sim \mid T - T_g(\phi) \mid^{\gamma(\phi)}$, where ϕ_g and T_g are, respectively, the value of ϕ and of T at the fluid-glass transition and γ is an exponent that is determined by the theory. The power-law fits for D as a function of $|T - T_g|$ and $|\phi - \phi_g|$ are shown in Fig. 1 (b) and (c). The power-law behavior of D allows us to trace the locus of points in the (ϕ,T) phase diagram for which $D = 0$ as shown in Fig. 1(b).

We then perform a bilinear transformation $T \to 0.575T + 0.059$, $\phi \to 1.03\phi + 0.049$ to superimpose the theoretical and the simulation line as reported in Fig. 1 (a), finding that the first A_4 is located at $(\phi^* = 0.6, T^* = 0.54)$. As stated above, the presence of an A_4 is signalled by a pure logarithmic behaviour of the density correlator at a given wave vector.

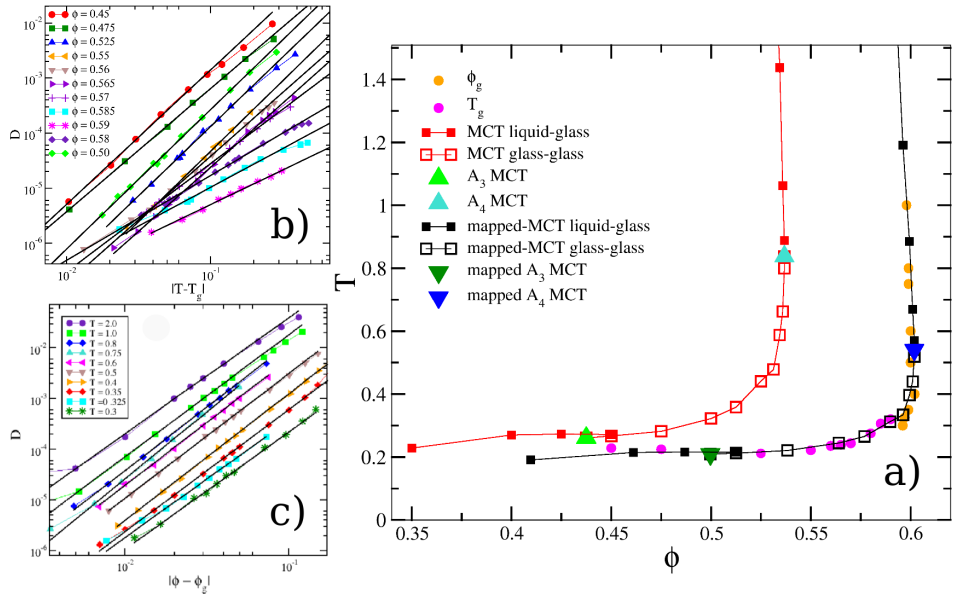

FIG. 1. (a) Fluid-glass and glass-glass transition line from MCT (red curve with open and filled symbols) obtained using as input the static structure factor evaluated from simulations.The magenta and orange filled circles are glass transition temperatures T_g and packing fractions ϕ_g extracted from a power-law fitting of the diffusivity D along isotherms and isochores respectively. A bilinear transformation in ϕ and T allows us to superimpose the theoretical data on the simulation results (black curve with open and filled symbols). (b) Diffusivity of species A, D as a funcion of $T - T_g$. (c)D as a function of $\phi - \phi_g$.

We have thus evaluated the density autocorrelation function of the A species $\Phi^{AA}_q(t)$ at different wave vectors q in a region of T and ϕ close to the estimated A_4, together with the mean square displacement (MSD) $\langle \delta r^2_{AA} \rangle$ as shown in Fig. 2 (a) and (b).

Notice that, at the expected state point we do not find any signature of an A_4 singularity. Instead the influence of the fluid-glass line controls the evolution of the two dynamic observables, thus hiding the presence of higher order singularities. In the present case, we observe the presence of an A_3 point, which lays in the glass region, but which can still influence the fluid states. As already found previously [1], the A_3 contribution to the dynamics can be observed only when the effect of the fluid glass-line on the fluid states is small. This is clearly shown in Fig. 2 where at $\phi = 0.585$ a logarithmic decay is found in $\Phi^{AA}_q(t)$, although for only two decades, and it gets progressively lost

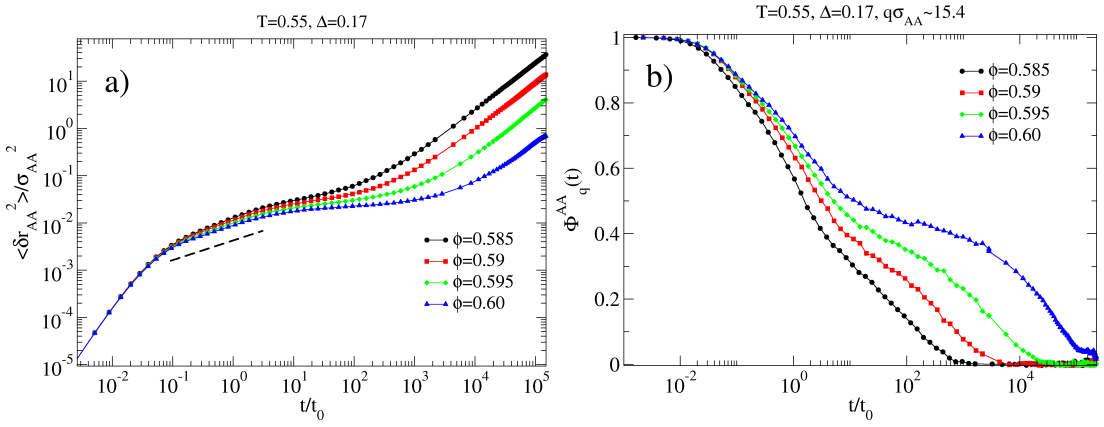

FIG. 2. a) MSD for the A particles at $T = 0.55$, $\Delta = 0.17$ and different ϕ. At the state point corresponding to the A_4 obtained by mapping the MCT fluid-glass line on to the simulation data, only a very weak influence of a higher order singularity can be observed. This is underlined by the dashed line which is a guide to the eye. b) density autocorrelation function $\Phi_q^{AA}(t)$ for the same state points of (a), for $q\sigma_{AA} \sim 15.4$ (the wave vector slightly changes depending on ϕ).

on increasing ϕ, similarly to what observed for $\Delta = 0.15$[1]. For such state point we have also evaluated $\Phi_q^{AA}(t)$ for different wave vectors $q\sigma_{AA}$ to show the typical concave-to-convex behaviour as illustrated in Fig.3. Since we find only A_3 features, we must increase Δ in order to find the A_4 singularity (following MCT predictions in Fig.1 of the manuscript). Indeed, we find such singularity for $\Delta \simeq 0.21$ as discussed in the manuscript.

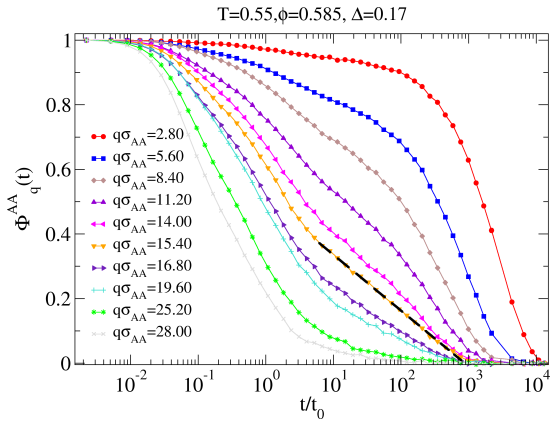

FIG. 3. density autocorrelation function $\Phi_q^{AA}(t)$ of the A species at $T = 0.55$,$\phi = 0.585$,$\Delta = 0.17$ for different wave vectors. At such ϕ, for $q\sigma_{AA} = 15.4$, the last part of the decay can be fitted with a pure logarithm, showing the presence of a higher-order singularity which is far from the given state point.

ENERGY AND STRUCTURE ALONG ISO-DYNAMICS LOCI

Here we show that while dynamics is invariant, thermodynamic and structural properties are not. Fig. 4 shows the structure factor $S(q)$ of a set of invariant points belonging to the $iso - D/D_0$ curve with $D/D_0 = 5.5 \times 10^{-5}$. Since the iso-dynamics points are very close to each other (there is only a difference of 4% in ϕ for the outermost points identified), $S(q)$ is very similar for all the state points, but we do observe a trend, e.g. in the growth of the first peak, which seems genuine within numerical resolution.

A stronger difference is observed by looking at the potential energy U along an iso-dynamics line. Since $U = \int dr g(r) u(r_{ij})$ (where, $u(r_{ij})$ is the pair potential and $g(r)$ is the radial distribution function), different U values imply a different structure for each point along the iso-dynamics line. Fig.5 shows the total potential energy for invariant points having $D/D_0 = 5.5 \times 10^{-5}$.

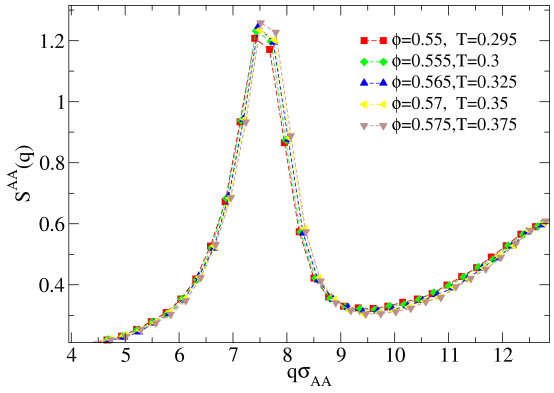

FIG. 4. Static structure factor for invariant point along the iso-D/D_0 with $D/D_0 = 5.5 \times 10^{-5}$ (squares).

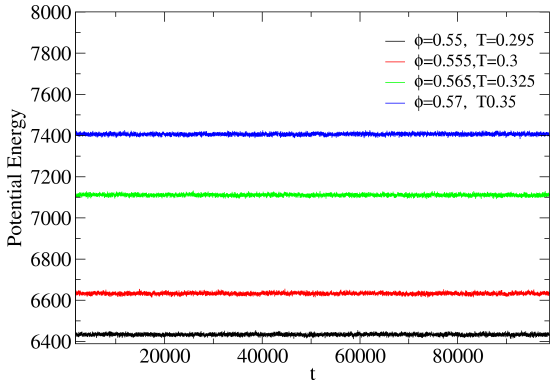

FIG. 5. Total potential energy for invariant point along the iso-D/D_0 with $D/D_0 = 5.5 \times 10^{-5}$ (squares).

ISO-DYNAMICS WITHIN MCT

While there is no general perturbative description for a classical fluid, it is the putative existence of MCT singularities that allows for such an analytical expansion. For both fluid-glass as well as higher-order singularities, such expansions involve the wave-vector dependent coefficients f_q, $H_q^{(1)}$, $H_q^{(2)}$ [2–4]. While these coefficients experience a regular dependence on the static structure, i.e. the external control parameters, they vary discontinuously at crossings of glass-transition lines which occur generically in the vicinity of higher-order singularities. As shown in [5], the higher-order singularities originate from a delicate balance of inner and outer shell of the potential: In between the higher-order singularities, the two contact values in the pair distribution functions $g(r)$ cause a beating in the static structure factor which gives rise to a strong enough additional contribution in the MCT vertex to trigger a line of glass-glass transition with endpoint singularities. It is important to notice that the two endpoints represent symmetric extreme representatives of such glass-glass transition points.

In between the endpoints but not outside, the glass-transition properties are generically very similar as shown for f_q in Fig. 6. Glass-form factors f_q are shown for several transition points in between the higher-order singularities as full curves together with two cases as dashed lines just outside the region. While the distributions outside vary from each other in a regular fashion, the distributions inside show very little variation. The situation is similar for the critical amplitude h_q in Fig. 7, and also in the same way behave values for the localization lengths, tagged-particle correlators, and other amplitudes.

The iso-dynamics lines do not extend all the way towards the higher-order singularities since at the higher-order singularities the dynamics is modified significantly from its well-known behavior by the critical exponents changing rapidly over a very narrow region of control parameters [3]. In between, the critical exponents a and b (the MCT exponent parameter λ), have a broad maximum (minimum). Hence, a generic reason for the iso-dynamics lines can be identified in the presence of two symmetric MCT endpoint singularities: The short-time dynamics is unaffected by

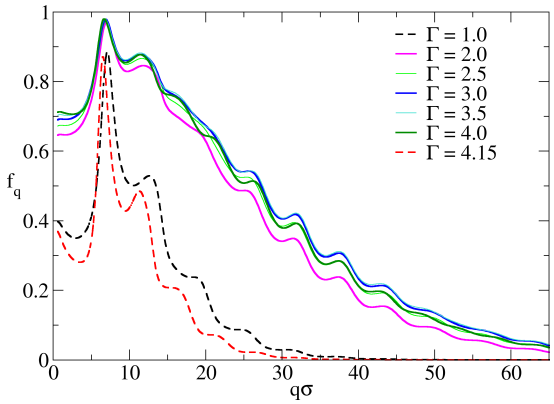

FIG. 6. Glass-form factors f_q along the transition line for $\Delta = 0.17$ and various values for the inverse temperature $\Gamma = 1/T$ calculated from MCT within RY, cf. [5]. The dashed curves represent transition points close to the higher-order singularities but *outside* the region of invariant dynamics. The full curves show the results for points spaced equally along the line *inside* the region of invariant dynamics.

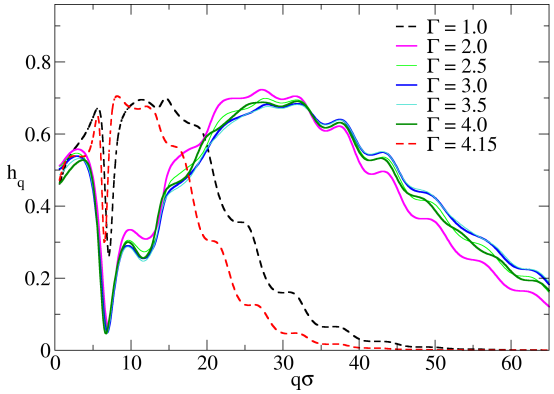

FIG. 7. Critical amplitudes h_q along the transition line for $\Delta = 0.17$ and various values for the inverse temperature $\Gamma = 1/T$ calculated from MCT within RY, cf. [5]. Line styles are identical to Fig. 6.

the presence of glass transitions and is therefore similar if the variation of the statics structure factors is small. The dynamics affected by the glass transitions experience especially little variation in the region of invariant dynamics since the variation of the critical parameters are restricted as explained above.

INDICATIONS FROM THE STATIC STRUCTURE

Within the MCT calculations it could be shown that the higher-order singularities originate from the competition of different wave-vector regimes in the static structure factor S_q where a beating phenomenon reflects the influence of inner and outer shell [5]. To support the conclusions drawn above within the MCT picture we show in Fig. 8 the static structure factor for the big particles: The contributions above the regular decay of $1/q^2$ for S_q towards its large-q limit of 0.5 are clearly seen to exhibit beating with a frequency characteristic of the distance of the two shells, $2\pi/\Delta \approx 37$. This beating frequency is observed most clearly between $q\sigma = 15$ and 45 while mixing effects may interfere at yet larger wave vectors and obscure the visibility of the beating. Finding the beating phenomenon in a region where also MCT effects regarding the higher-order singularities are most prominent lends further support to the interpretation of our data within the MCT predictions.

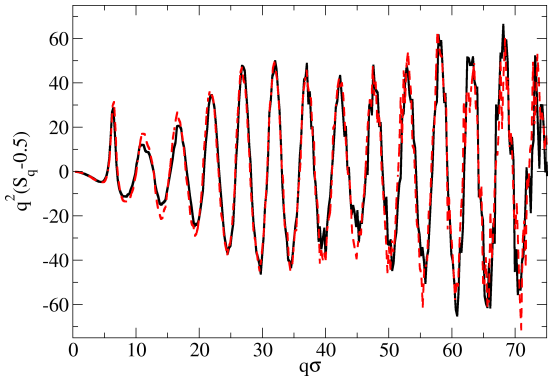

FIG. 8. Static structure factor for large wave vectors plotted as $q^2(S_q - 0.5)$ for $\Delta = 0.17$ and $(\varphi, T) = (0.55, 0.295)$ as full and (0.58, 0.425) as dashed curve.

[1] G. Das, N. Gnan, F. Sciortino and E. Zaccarelli, J. Chem. Phys. **138**, 134501 (2013).
[2] T. Franosch, M. Fuchs, W. Götze, M. R. Mayr, and A. P. Singh, Phys. Rev. E **55** 7153 (1997).
[3] W. Götze and M. Sperl, Phys. Rev. E **66**, 011405 (2002).
[4] F. Sciortino, P. Tartaglia, E. Zaccarelli, Phys. Rev. Lett. **91**, 268301 (2003).
[5] M. Sperl, E. Zaccarelli, F. Sciortino, P. Kumar, H. E. Stanley, Phys. Rev. Lett. **104**, 145701 (2010).